Hyperthermic effect of magnetic nanoparticles under electromagnetic field

Giovanni Baldi*, Giada Lorenzi, Costanza Ravagli

Centro Ricerche Colorobbia, Sovigliana - Vinci, Florence, 50053, Italy

Received 11 April 2009; received in revised form 3 June 2009; accepted 10 June 2009

Abstract

Magnetic nanoparticles have attracted increasingly attention due to their potential applications in many industrial fields, even extending their use in biomedical applications. In the latter contest the main features of magnetic nanoparticles are the possibility to be driven by external magnetic fields, the ability to pass through capillaries without occluding them and to absorb and convert electromagnetic radiation in to heat (Magnetic Fluid Hyperthermia). The main challenges of the current works on hyperthermia deal with the achievement of highly efficiency magnetic nanoparticles, the surface grafting with ligands able to facilitate their specific internalisation in tumour cells and the design of stealth nanocomposites able to circulate in the blood compartment for a long time. This article presents the synthesis of cobalt ferrite nanoparticles dispersed in diethylene glycol via the so called polyol strategy and the crystal size control through successive synthesis steps. Preliminary heat dissipation evaluations on the prepared samples were carried out and the question of how particles sizes affect their magnetic and hyperthermic properties was addressed as well. Furthermore we will present how surface chemistry can be modified in order to change the dispersity of the product without affecting magnetic and hyperthermic properties.

Keywords*: cobalt ferrite; magnetic nanoparticles; hyperthermia; polyol synthesis*

I. Introduction

The nanotechnology is currently the focus of intense development in the field of nanomedicine. Nanometer-sized particles, such as biodegradable micelles, semiconductor quantum dots and iron oxide nanocrystals, have functional or structural properties that are not available from other existing molecular or macroscopic agents. Recent advances in nanotechnology have led towards the development of multifunctional nanoparticle probes for molecular and cellular imaging, nanoparticle drugs for targeted therapy, and integrated nanocarriers for early cancer detection and screening [1–3]. As these multifunctional nanocarriers have the ability to act both as diagnostic tools for tumour detection and as a therapeutic biocarriers, they allow to define a new nanoparticle based technology for simultaneous diagnosis of different cancers and therapeutics (Theranostics). Concerning magnetic nanoparticles, the main advantage in their employment in nanomedicine is that they can be visualized in Magnetic Resonance Imaging (MRI) techniques acting therefore as magnetic contrast agents (CA). In addition, their ability of self heating when irradiated by electromagnetic field in the range of kHz–MHz is expected to provide a great deal of technical advantages, accelerating a new form of therapeutic hyperthermia cancer treatment, the so-called Magnetic Fluid Hyperthermia (MFH) [4]. Organic materials, as living tissues or certain polymers absorb electromagnetic radiation due to the presence of electrical dipoles (permanent or induced) that couples with the electrical vector of the radiation (dielectric heating) inducing rotation of the absorbing dipole that generate heat by friction. In this kind of hyperthermia the electromagnetic radiation is usually in the range of GHz. In Magnetic Fluid Hyperthermia the principle is similar but in this case the magnetic moment of the particles interacts with the magnetic vector of the electromagnetic radiation. In MFH the size of the magnetic material exposed to the EM radiation is crucial as the magnetism of massive ma-

* Corresponding author: tel: +39 0571 709758
fax: +39 0571 709875, e-mail: *baldig@colorobbia.it*

terials and nanoparticles is completely different. In the first case heat dissipation occurs due to the material intrinsic hysteresis energy losses, while in the second one particles heating is caused by relaxation phenomena both of particles magnetic moments following the electromagnetic field and of the mechanical rotation of particles themselves within the dispersant medium [4]. Experimental evidence shows that magnetic nanoparticles are more efficient than their massive counterparts in hyperthermia applications [5], and therefore it is of paramount importance to control particles size in order to maximize the efficiency for this specific application.

Iron oxide nanoparticles are already in use for cell separation and purification and as contrast agents for magnetic resonance imaging (MRI) and are currently under investigation for several other applications, including drug delivery, nanobiosensors, and magnetic fluid hyperthermia [6]. Up to now the research attention has been essentially restricted to iron oxide-based materials, mainly because they are easily prepared, are biodegradable and biocompatible and can thus be recycled by cells using normal biochemical pathways for iron metabolism. On the other hand, since the magnetocrystalline anisotropy of a single domain magnetic particle is strictly connected to its hyperthermic efficiency, the use of different materials with larger magnetic anisotropy and larger magnetic moment, such as cobalt ferrite $CoFe_2O_4$, is strongly envisaged since it can allow a significant improvement of the material efficiency, particularly as concerns MFH and MRI. Moreover, the use of such materials may allow reducing the particle size introducing additional benefits, as longer half-life time in the blood with consequently increased taken up by the reticulo-endothelial system and minor inorganic dose, thus reducing particles potential toxicity.

Measurements of the heat generation by magnetic particles under AC magnetic field (i.e. MFH) are usually quoted in terms of the Specific Absorption Rate (SAR), also denoted *specific loss power* (SLP), which is operatively defined as the heating power of a magnetic material per unit mass. For clinical purposes, the value of SAR is crucial because the higher the specific absorption rate, the lower the injected dose to the patient. Concerning the electromagnetic devices used for magnetic hyperthermia evaluation, the technology is still under development. Most magnetic hyperthermia experiments are done with laboratory-made generators in the frequency range of 50 kHz-1 MHz, with magnetic field amplitudes up to a few tens of kA/m [7]. They are mostly performed in an induction coil or in the air-gap of a magnetic inductor, cooled by water or air.

In this fascinating scientific framework, our group has successfully attained in the production of several spinel ferrites in the form of stable dispersions. In particular, the synthesis of $CoFe_2O_4$ nanoparticles has been scaled to 20 L production. The technique is based on the polyol-mediated synthesis which allows to finely tune the average size of the particles in the 5–10 nm range. Moreover, modification of the particles dispersity was carried out by replacing the solvent coating with proper ligands, demonstrating the easiness of surface engineering as a step towards biomedical device assembly.

A proof of concept experimentation of magnetic heating of nanoparticles under AC magnetic field was carried out with a home-made magnetothermal set-up, properly tuned in order to minimize heat losses with environment. The hyperthermic efficiency of different-size cobalt ferrite samples was tested by evaluating SAR under AC field irradiation, and the preliminary results achieved were finally correlated with the main magnetostatic and morphological properties of the samples investigated.

II. Experimental

2.1 Synthesis

Ferric acetate, ($Fe(CH_3COO)_3 \cdot xH_2O$) was purchased from The Shepherd Chemical Company. The iron content was evaluated by ICP-AES to be 26 wt.%. Cobalt Acetate ($Co(CH_3COO)_2 \cdot 4H_2O$, 23.7 wt.% in Co) was bought from OMG Kokkola Chemicals and diethylene glycol (DEG = $O(CH_2CH_2OH)_2$) from Chimica Corona. Potassium 1-hexadecanol phosphate for particle coating was purchased by Roche. Polyethylene glycol with average molecular mass of 10.000 Da (PEG 10.000) and paraffin wax (m.p. 65°C) for particles embedding in an inert matrix were purchased from Merck and Sigma-Aldrich, respectively. All the chemicals were of reagent grade and were used without any further purification.

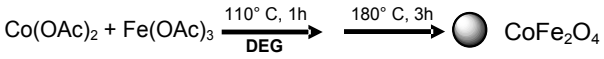

Scheme 1. Synthesis of cobalt ferrite nanoparticles using the polyol-mediated technique

Cobalt ferrite nanoparticles (the sample CoFe1, see Table 1) were synthesised with the following polyol method [8,9]: cobalt and iron acetates (89.6 and 179.2 mmol, respectively) were solubilised in 645 g of diethylene glycol at 110°C for one hour. The solution was successively heated to 180°C with a heating rate of 2°C/min and then kept at 180°C for three hours. After this growing period the dispersion has been air cooled to room temperature and stored (Scheme 1). The final concentration of cobalt ferrite, as evaluated from ICP-AES, resulted equal to 2.88%. A second series of ferrite particles with larger average size, (the samples CoFe2-6), was prepared as follows: we synthesised cobalt ferrite nanoparticles, the sample CoFe2, as described above using half concentrations of acetates with respect to

Table 1. Main structural, magnetic and hyperthermic features for the prepared cobalt ferrite samples

Sample	Concentration [wt.%]	Fe/Co molar ratio	D_{XRD} [nm]	D_{DLS} [nm]	PDI	T_B [K]	SAR [W/g]
CoFe1	2.88	2.20	5.5	12.4	0.19	199	76.7
CoFe2	1.57	2.24	5.0	5.46	0.19	177	-
CoFe3	3.13	2.15	5.9	7.26	0.18	188.8	105
CoFe4	3.17	2.26	6.0	11.2	0.19	213	153
CoFe5	3.40	2.20	6.2	13.2	0.23	265.5	188
CoFe6	3.26	2.18	6.7	18.9	0.21	289	250
CoFe7	-	-	5.5	12.6	0.13	195	-

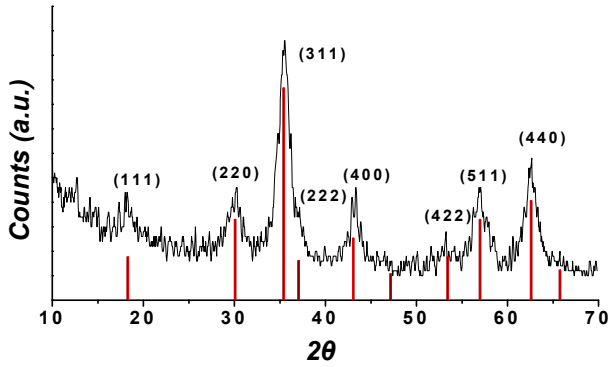

Figure 1. Powder X-ray diffraction pattern of CoFe1 and reference pattern for $CoFe_2O_4$. Evaluation of the particle size by using the Scherrer formula gave an average diameter of 5.5 nm

the sample CoFe1 (the final concentration of cobalt ferrite was 1.5 wt.%). After the first synthesis step, suitable quantities of solvent and precursors were added at room temperature to keep the final magnetic material concentration at 3 wt.% and the heating cycle was repeated (1 hour at 110°C and 3 hours at 180°C) in order to obtain larger particles (the sample CoFe3). Repeating the same procedure three times, using each time particles prepared in the previous step as initial seeds, yielded samples CoFe4, CoFe5 and CoFe6. These synthetic procedures can be easily scaled up to a 20 L pilot plant without major differences in morphological and magnetic properties.

Coating of CoFe1 particles (the sample CoFe7), were achieved by dissolving 1.7 mmol of cethyl phosphate in 20 g of ethanol and gently heating when needed. After complete solubilisation, 10 g of the dispersion CoFe1 were added drop wise to the ethanol solution and kept under vigorous stirring for one hour. Successively 40 g of n-hexane were added to the solution, and after 30 minutes under stirring, the two phases were separated with a separator funnel.

In order to mechanically block the particles, 5 wt.% of the sample CoFe1 was added to polyethylene glycol (average molecular weight 10.000 Da) heated at 80°C and kept under stirring for 1 hour (PEG 10.000 has a melting temperature in the 58–63°C range). After complete mixing the product has been rapidly cooled in order to entrap the nanoparticles in the solidifying PEG.

Dispersions in solid paraffin of the sample CoFe7 were obtained in a similar way by mixing paraffin (melting point 65°C) with the hexane dispersion at 80°C and then cooling after solvent evaporation. ICP analysis gave concentration of 0.15 wt.%.

2.2 Chemical and physical characterisation.

Cobalt and iron concentrations of the samples were measured after dissolution of the samples in concentrated nitric acid, the measurement were carried out by solution nebulisation inductively coupled plasma emission spectrometry (ICP-AES, Varian Liberty 51). Morphological evaluations were carried out with Dynamic Light Scattering (DLS) measurements performed on 1 $g_{CoFe2O4}/dm^3$ in a quartz cuvette on a Malvern Zetasizer nano-S working with a 532 nm laser beam. STEM images have been recorded using an Oxford ZEISS Supra40 high resolution FESEM operating at 20 KV, with a resolution of 1.0 nm. Samples were deposited on FESEM carbon coated copper grids after proper UP water dilution (~ $5 \cdot 10^{-4}$ wt.%). The crystalline structure of the samples was identified from X-ray diffraction (XRD) patterns recorded in the 2θ range 10–70° with a scan step of 0.05°(2θ) for 5 s on a Philips X'pert pro diffractometer (Cu K_α radiation). The crystallite size was determined from the (311) diffraction peak by using the Scherrer method.

2.3 Magnetic characterisation

Magnetic measurements were performed with a S600 SQUID magnetometer from Cryogenic Ltd. and with an Oxford VSM on solid, PEG-embedded samples.

2.4 Hyperthermic measurements

Preliminary hyperthermia efficiency tests were performed on cobalt ferrite samples with a Nova Star 5kW® equipment purchased by Ameritherm Inc. The sample was irradiated for 300 s by an alternating magnetic field of 21 kA/m with a varying frequency of 167 kHz. The heating equipment was set at the proper field intensity by adjusting the voltage in the power supply, while the frequency was varied by properly setting the copper coil (total length of 73 mm with 9 turns and ∅ = 50 mm) and the inductors (0.33 μF). The temper-

ature increase was recorded both with IR Thermacam® (FLIR Thermacam E65, FLIR Systems, Boston, MA, USA) and with a digital temperature recorder (VR18_CR®, by Ceam Group) connected to an optical fibre directly dipped into the sample.

III. Results and discussion

The reaction consists of a high temperature hydrolysis in which the acetic acid produced during the reaction is distilled leaving a stable dispersion of the inorganic material in the solvent. It must be noted that the final dispersion has low ionic strength and low dielectric constant that justify dispersion stability (see below). The XRD pattern (Fig. 1) of the dried CoFe1 sample matches the one expected for the spinel phase characteristic of cobalt ferrite. The average crystallite size was estimated from the X-ray diffraction line broadening measurement by using the Scherrer formula. The analysis of the (311) peak gave a mean diameter of 5.5 nm.

Dynamic light scattering measurement of the sample CoFe1 in DEG (Fig. 2) revealed a uniform dispersion of nanoparticles (PDI < 0.1) with average diameter of 12.4 nm. DLS measurements on the sample CoFe1 over a two years period did not show any significant alteration of the dispersion stability. This can be addressed, according to the DLVO theory, to the low ionic strength and consequently low dielectric constant of the final dispersion, that determines a thick electrical double layer that increases the repulsive forces between the charged particles preventing agglomeration.

In Fig. 3 a SEM image of the dispersion of CoFe1 in ethanol deposited over a Cu grid, is shown. The sample consists of a uniform dispersion of spherical particles with a quite narrow size distribution and a mean diameter of 5.8 nm. The obtained value is close to that obtained from XRD measurements indicating a high crystalline degree of all the particles. The well visible shell surrounding the particles can be ascribed to the solvent coordinating around particles surface. A similar structural and morphological characterisation was performed on the other samples, CoFe2-6, produced with the seed approach. The main structural features obtained are listed in Table 1 and the increase of the hydrodynamic diameter with the synthesis step is shown in Fig. 4.

The data show that the proposed synthetic method is effective for producing high crystalline cobalt ferrite nanoparticles with increasing crystal sizes in the 5–7 nm. For all samples the observed Co/Fe molar ratio is constant and close to that of stoichiometric $CoFe_2O_4$. The difference with the value obtained by DLS arises from the analytical techniques used, which provides information on the size of the diffracting nanocrystals (XRD) and on the hydrodynamic diameter of the scattering object including the eventual amorphous surface layer and the solvatation sphere (DLS).

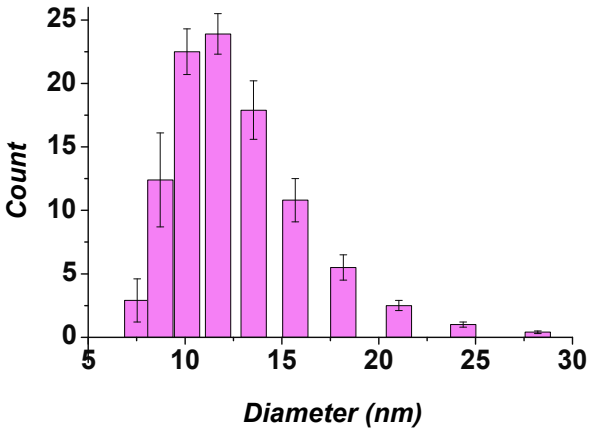

Figure 2. Size histograms of suspensions of CoFe1 obtained from DLS measurements. The sample was dispersed in DEG

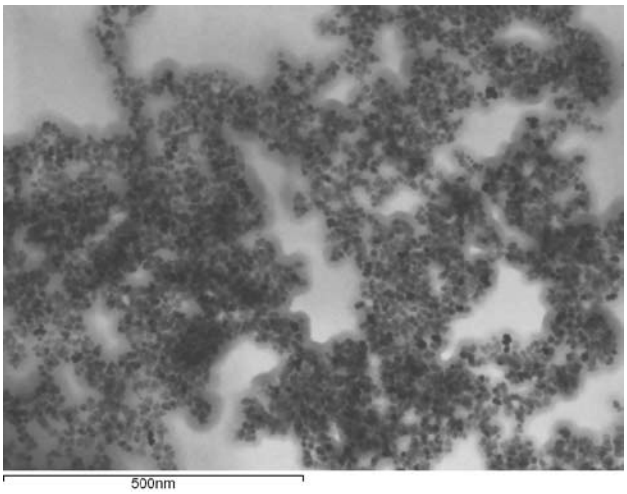

Figure 3. STEM image of sample CoFe1 dispersed in ethanol

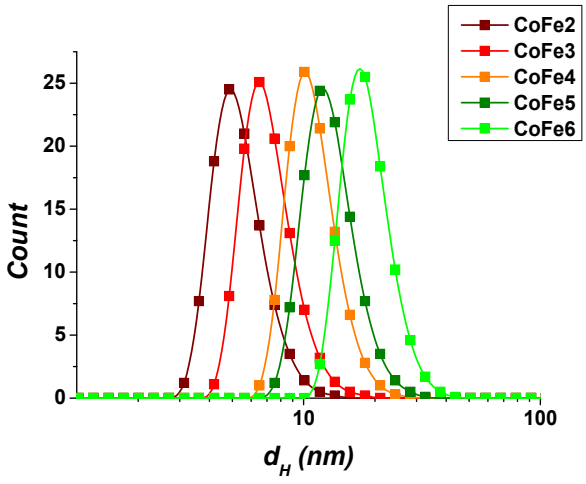

Figure 4. Hydrodynamic diameter increase observed with DLS measurements on samples CoFe2-6

In order to investigate the change of particles dispersity we covered cobalt ferrite nanoparticles, the sample CoFe1, with hexadecanol phosphate. The thermal analysis of the dry coated particles confirmed that the ligand replacement occurred quantitatively giving an uptake of 33.8% [10]. As a consequence the dispersity character was observed to change from hydrophilic to hydrophobic, as a result the sample forms a stable hexane dispersion. DLS measurement in hexane (Table 1) of the sample CoFe7 showed that also in this case particles are well dispersed and the suspension is stable over a long time period.

Zero-Field-Cooled (ZFC) and Field-Cooled (FC) magnetisation curves, were recorded for samples CoFe2-7 by applying a probe field of 50 Oe, in the temperature range 2.5–300 K. All the measurements were performed on particle solid dispersions, in PEG for the uncoated particles and paraffin wax for the organic-coated sample CoFe7. In Fig. 5 are reported the ZFC-FC curves for the samples CoFe2-6. As expected for a size-spread collection of superparamagnetic particles, the ZFC curves show a peak, whose maximum is commonly associated to the mean blocking temperature of the assembly, T_B, i.e. the temperature at which the relaxation time of the magnetisation equals the characteristic time of the measurement. The mean blocking temperature T_B clearly increases with increasing particle size, from 177 K for the sample CoFe2 up to 298 K for the sample CoFe6 (Table 1). It is worthwhile to note that, thanks to the large value of the anisotropy constant of cobalt ferrite ($K \sim 1.2$ MJ/m^3) [8], even a small change in the particle size produces a significant modification of the magnetic properties related to the magnetisation relaxation. Indeed, for not interacting single domain particles the relaxation of the magnetic moment can be described by the Néel model which predicts an Arrhenius law:

$$\tau = \tau_0 \exp(KV/k_BT) \quad (1)$$

where τ is the Néel relaxation time, K the anisotropy constant, V is the particle volume and τ_0 the attempt time. According to the theory of magnetic hyperthermia [4] the power dissipated by a ferrofluid during the AC field irradiation, given by:

$$P = \mu_0 \pi \chi''(\tau) f H_0^2 \quad (2)$$

is directly proportional to the value of χ'', the imaginary part of susceptibility, which can be expressed by the Debye relationship:

$$\chi'' = \chi_0 \frac{\omega\tau}{1+(\omega\tau)^2} \quad (3)$$

being χ'' function of τ, the relaxation time for magnetization reversal. It follows that the hyperthermic efficiency of an assembly of single domain magnetic nanoparticles is strictly dependent on τ, which, in turn, is exponentially dependent on K, according to equation (1).

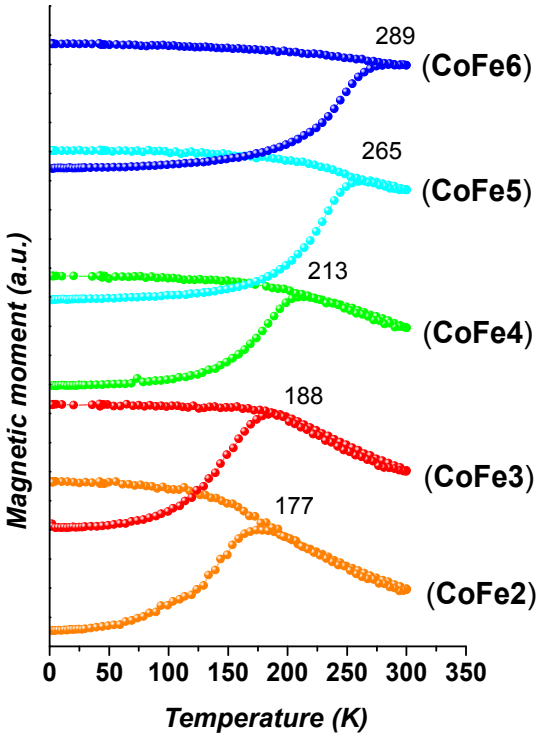

Figure 5. ZFC and FC magnetizations as a function of temperature for samples CoFe2-6 in PEG measured applying a magnetic field of 4 kA/m. They are vertically shifted for a better presentation

Hyperthermic experiments were carried out at 298 K; in preliminary studies investigations on the field homogeneity and the temperature gradients within the sample were performed. The images were collected every 60 seconds with IR Thermacam®. The differences in the heating of the ferrofluid along the length (z axis) of the coil are reported in the graph in Fig. 6. As we can see, even a small deviation from the central position of the sample under measurement results in a less intense magnetic field irradiation. With regard to the field ho-

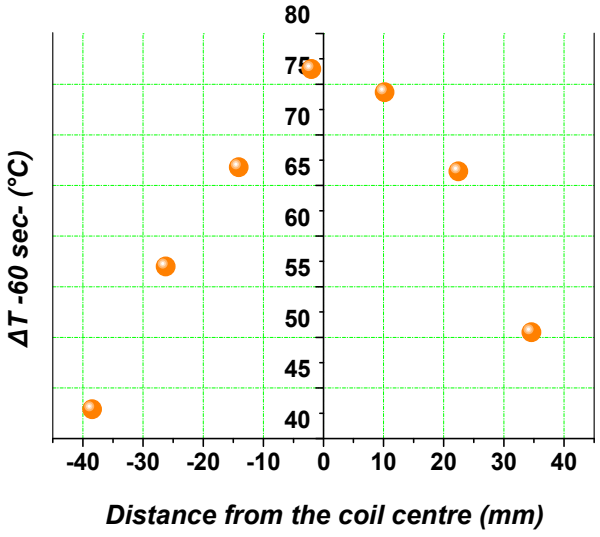

Figure 6. Temperature increase after 60 s irradiation as function of the distance from the centre of the coil

τ

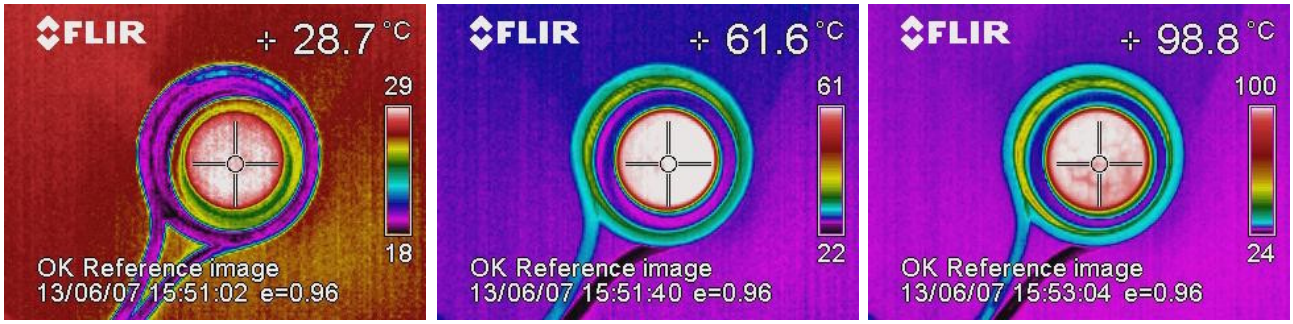

Figure 7. Thermal images of a $CoFe_2O_4$ sample within a Petri capsule at 0 s, 30 s and 60 s during AC field irradiation, respectively from the left

mogeneity on the *xy* plane, the images taken with the sample at the z-centre of the coil reveal the absence of any temperature gradient after 30 seconds of irradiation, and a little cooling at the boundaries of the capsule after 60 seconds of irradiation, probably due to the quick heat exchange between the large sample surface and the environment at temperatures around 100°C (Fig. 7)

In order to avoid as much as possible heat exchange between the sample and the external environment, samples SAR was evaluated by measuring the temperature raise of the dispersion during AC magnetic field irradiation with an optical fibre probe directly dipped into the sample.

The specific absorption rate is defined as the total heat dissipated by the sample divided by the total mass of metal and the irradiation time:

$$SAR = \frac{\sum_i m_i C_{pi}}{m_{Metal}} \cdot \Delta T / \Delta t \qquad (4)$$

with i every species involved in heat exchange, m the mass in grams of each material, C_p their specific heat capacity [J/K·g] and m_{Me} the total mass of metal. We extrapolated the value of $\Delta T/\Delta t$ at $t \rightarrow 0$ to minimize the unquantifiable heat exchange contributions of the sample with the environment, calculating the value of the initial linear rise in temperature versus time with a simple differentiation of the experimental curve. The results, shown in Fig. 8 and reported in Table 1, indicate that the hyperthermic efficiency increases with particle size and synthesis steps. As expected from the theory, equations (1-3), SAR values obtained by the initial temperature rise show a strong dependence on particles size, varying from 77 [W/g] up to 250 [W/g], by less than 2.0 nm increase of the mean crystalline size. Moreover, thanks to the extremely enhanced value of cobalt ferrite anisotropy constant, even a small size change remarkably affects the energy barrier for magnetisation reversal, equation (1). Therefore, we suggest that the increase of the hyperthermic efficiency with size should be mainly related to the dependence of SAR on magnetisation relaxation phenomena of particles under the AC field, according to equation (2).

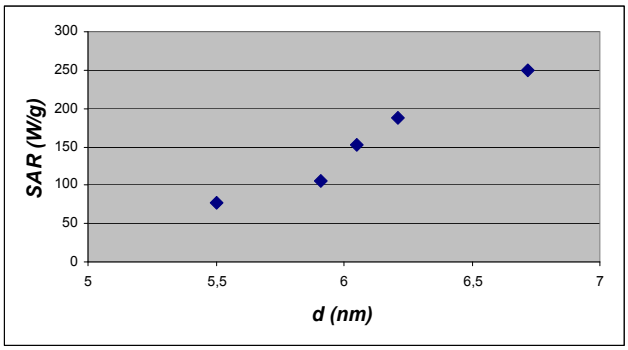

Figure 8. Hyperthermic efficiency of cobalt ferrite samples as function of the crystalline diameter

The magnetic properties of the functionalised particles were also investigated. The mean blocking temperature of samples CoFe1 and CoFe7 (Table 1) do not differ appreciably indicating that the ligand exchange does not significantly affect the magnetic behaviour and thus that the chemical state of surface ions has not a relevant role in the determination of the magnetic properties.

IV. Conclusions

A novel method to prepare spherical shaped, highly monodisperse, spinel ferrite $CoFe_2O_4$ nanoparticles, in the form of stable dispersion is presented. The technique is based on the polyol synthesis and can be repeated in subsequent steps, using each time ferrite particles as seed, to finely tune the average size of the particles in the 5–7 nm range. Modification of the particle dispersity was successfully attained by replacing the coating with proper ligands demonstrating the easiness of surface engineering, permitting not only solvent changes (of technological importance) but also representing a first step towards biomedical device assemblies. Due to the large anisotropy of the considered material, a small variation in the average volume produces a dramatic increase of the energy barrier for magnetisation reversal from 177 K for the sample CoFe2 to room temperature for the sample CoFe6 with largest particles. This effect is supposed to be responsible for the large increase in hyperthermic efficiency with particles size. Fine tuning of nanoparticle size leads to an increase in material hyperthermic efficiency that is critical for both producing higher local temperatures and also reducing the quantities of

the material needed to achieve a target temperature, of paramount importance in biomedical applications. For biomedical applications a biocompatible coverage of the particles has to be provided in order to avoid immunodefensive system reactions, moreover successive anchoring of targeting moieties can direct the particles to a specified target as a following step. In this sense we are currently developing new biocompatible hyperthrmic nanoparticles in order to provide an alternative strategy in the cure of cancer.

Aknowledgements: The authors wish to thank Dr. Claudio Sangregorio and Dr. Claudia Innocenti (LAMM, Laboratory of Molecular Magnetism, INSTM, Florence, Italy) for magnetic measurements, Dr. Daniele Bonacchi for his research support and Dr. Mauro Comes Franchini (University of Bologna, Italy) for the investigations on organic coating of nanoparticles.

References

1. J. Kreuter, R.N. Alyautdin, D.A. Kharkevich, A.A. Ivanov, "Passage of peptides through the blood-brain barrier with colloidal polymer particles (nanoparticles)", *Brain Res.*, **674** [1] (1995) 171–174.
2. M. Lewin, N. Carlesso, C.H. Tung, X.W. Tang, D. Cory, D.T. Scadden, R. Weissleder, "Tat peptide-derivatized magnetic nanoparticles allow in vivo tracking and recovery of progenitor cells", *Nature Biotechnol.*, **18** (2000) 410–414.
3. Y. Anzai, K.E. Blackwell, S.L. Hirschowitz, J.W. Rogers, Y. Sato, W.T. Yuh, V.M. Runge, M.R. Morris, S.J. McLachlan, R.B. Lufkin, "Initial clinical experience with dextran-coated superparamagnetic iron oxide for detection of lymph node metastases in patients with head and neck cancer", *Radiology*, **192** (1994) 709–715.
4. R.E. Rosenweig, "Heating magnetic fluids with alternating magnetic field", *J. Magn. Magn. Mater.*, **252** (2002) 370–374.
5. R. Hergt, W. Andrä, C.G. d´Ambly, I. Hilger, W.A. Kaiser, U. Richter, H.G. Schmidt, "Physical limits of hyperthermia using magnetite fine particles", *IEEE Trans. Magn.*, **34** (1998) 3745–3754.
6. A.K. Gupta, M. Gupta, "Synthesis and surface engineering of iron oxide nanoparticles for biomedical applications", *Biomater.*, **26** (2005) 3995–4021.
7. S. Mornet, S. Vasseur, F. Grasset, E. Duguet, "Magnetic nanoparticles and their applications in medicine", *J. Mater. Chem.*, **14** (2004) 2161–2175.
8. G. Baldi, D. Bonacchi, C. Innocenti, G. Lorenzi, C. Sangregorio, "Cobalt ferrite nanoparticles: The control of the particle size and surface state and their effects on magnetic properties", *J. Magn. Magn. Mater.*, **311** (2007) 10–16.
9. G. Baldi, A. Barzanti, M. Bitossi, PCT EP03/02281, 2002.
10. G. Baldi, D. Bonacchi, M. Comes Franchini, D. Gentili, G. Lorenzi, A. Ricci, C. Ravagli, "Synthesis and coating of cobalt ferrite nanoparticles. A first step towards the obtainment of new magnetic nanocarriers" *Langmuir*, **23** (2007) 4026–4028.